Hybrid Technique for Estimating Fetal Head Circumference Using Ultrasound Imaging

Ameera Shafique[1], Zobia Suhail[1], and Hafiz Muhammad Danish[2]
[1]Department of Computer Science, Faculty of Computing and Information Technology, University of the Punjab, Lahore, Pakistan.
[2]Department of Computer Science, University of Engineering and Technology, New Campus, Lahore, Pakistan.
* Correspondence: Ameera Shafique (mscsf21m518@pucit.edu.pk).

Citation | Shafique. A, Suhail. Z, Danish. H. M, "Fetal Head Circumference Estimation Using Sonographic Images", IJIST, Vol. 6 Issue. 3 pp 1058-1075, July 2024
DOI | https://doi.org/10.33411/ijist/20246310581075
Received | July 03, 2024 **Revised |** July 25, 2024 **Accepted |** June 28, 2024 **Published |** July 30, 2024.

Abstract.
Introduction: Analysis of fetal head shape is crucial for assessing head growth and detecting abnormalities in fetuses. In traditional clinical practice, Head Circumference (HC) is determined by manually fitting an ellipse to the fetal skull based on 2D ultrasound images.
Novelty Statement: To address this, an automated method integrating image processing techniques with U-net variant have been developed to achieve maximum accuracy of fetal head circumference detection on HC18 dataset. This method aims to enhance precision in HC delineation, thereby improving clinical reliability.
Material and Method: This study proposed a method that combines image processing techniques (noise removal, edge detection, segmentation) with a Residual U-net model for detecting the boundary of the fetal skull using HC18 dataset.
Results and Discussion: The results of this method outperformed a simple residual u-net model in terms of accuracy. The proposed method is evaluating using the HC18 challenge dataset, achieving a Dice coefficient of 97.99%, a mean difference of 5.86 mm, and a mean Hausdorff distance of 0.56 mm compared to manual annotations. These results demonstrate the effectiveness of the proposed method in accurately delineating the fetal skull boundary.
Concluding remarks: Furthermore, the proposed method shows comparability with state-of-the-art techniques in the field.

Keywords: Ultrasound, Imposed images, Head circumference, Residua U-net.

Introduction:

Fetal biometric ultrasound measurements are routinely conducted manually by healthcare professionals using ultrasound machines. Compared to CT scans and MRI, ultrasound is efficient, safe, and less expensive. It uses low-volume sound waves, minimizing the risk of miscarriage or harm to both the patient and fetus [1]. During the ultrasound examination, the operator manually draws lines and circles on the ultrasound images using a cursor or caliper. A fetus is an unhatched or unborn vertebrate, particularly after it has developed its basic structure. Monitoring fetal growth is crucial for assessing fetus's general health and well-being. Several measurements, including parietal diameter, abdominal circumference, femoral length, and head circumference, are performed regularly to estimate fetal growth. However, these manual measurements can cause errors and wrong values due to acoustic shadows, discontinuous anatomic boundaries, speckle noise, and low contrast, which can complicate the boundary detection process.

Professionals calculate gestational age and fetal weight using specific mathematical functions, which are time-consuming and operator-dependent [2] [3]. To overcome these challenges, an automatic system for segmentation and measurement of fetal biometrics is needed to facilitate such processes and aid in the analysis of results. Such a system would optimize results, improve performance, and reduce human error. In our proposed method, we utilized ultrasound images and applied image processing techniques to eliminate noise and isolate the region corresponding to the fetal head. By integrating these techniques with deep learning models, our objective is to achieve precise and reliable measurements. Our ultimate aim is to create an algorithm that can automatically compute the circumference of the fetal head using a 2D ultrasound images in HC18 dataset [4]. This innovative approach not only enhances efficiency but also ensures consistent data acquisition, which is of utmost importance in clinical ultrasound diagnostics for accurately quantifying anatomical structures.

Objectives:

The aim of this work is to achieve maximum accuracy on HC18 dataset by enhancing ultrasound images using image processing techniques to eliminate noise and isolate the region corresponding to the fetal head and then collaborate the results with predefined variant of U-net model.

Novelty Statement:

The main contribution of this work is to achieve 97.99% of dice coefficient which is highest from the other U-net variants applied on the same dataset before. This is achieved by applying various image processing methods to eliminate noise and segmented the fetal head we refined Sonographic images before passing it into model's training phase. Then apply variant of U-net model, Residual U-net which is never used before in HC18 competition to achieve precise and reliable circumference measurements than simple Residual U-net. We visually compare their performance and evaluate them using metrics provided by the HC18 dataset discussed in section, demonstrating the significance and accuracy of our proposed method.

This paper is structured as follows: Section 2 provides a concise overview of the related work. Section 3 outlines the materials and methods used in the study. In Section 4, we present a detailed analysis of experimental results and comparative findings. Finally, we conclude with the key insights derived from this research.

Related Work:

In the past, many authors proposed solutions to solve this problem utilizing various techniques in medical image processing, deep learning, and machine learning. These techniques and solutions have different impacts and accuracy rates which are discussed in this section. R. Ramya et al [5] applied binary thresholding to segment the image and ellipse fitting for calculating head circumference. In [6] Monica R et al conducted an assessment of fetal growth; they apply different noise removal filters and find Lee is the best. Morphology,

thinning, and ellipse fitting techniques are used and they achieved 92% of accuracy. In [7], Mathews M et al segmented the fetal head by using two approaches chamfer Matching and Hough Transform. They achieved 95.55% and 91.11% accuracy respectively. Wei Lu et al [8] used iterative randomized Hough transform, K-Mean, and morphological operation for head detection. Ketheesan Thirusittampalam et al [9] employed CNN with a U-net model for feature extraction and classification. They first localized the head region and then fit the ellipse for head segmentation resulting in 100% accuracy of localization and 88.96% specification. In [10] Changming Sun presented a circular shortest path technique for fetal head measurement, applying CSP extraction using branch and bound, and ellipse fitting to identify the head shape. Gennady V.Ponomarevet et al [11] worked on fetal head measurement by using multilevel thresholding and shape-based recognition and applying possible combinations of the ellipse to find head contour with 96.6% accuracy. In [12] Valiollah Salari et al applied thresholding, gradient operator, and least square method for head detection. Yufei Shen et al [13] used an Iterative randomized Hough transform approach, adaptive threshold, and morphology thinning operation. In [14] Rong Xu et al employed an Iterative randomized hough transform approach with bilateral filter, top hat morphology operation, and k-means segmentation. W.FathimaFarsana et al [15] proposed a random forest classifier for the detected region of interest by using a pyramid histogram of oriented gradients. Lei Zhang et al [16] proposed a texton-based method that then trains a random forest model resulting in 95.24% of overall accuracy. Khusnul Danny Rahayu et al [17] used a Gaussian filter and canny edge detection for edge extraction, and contour technique to detect fetal head with an accuracy of 97.77%.

Baidaa Al-Bander et al [18] used a deep learning technique, extracting features using a convolutional neural network with ResNet101 as the backbone architecture. Faster R-CNN was applied for object localization and then passed to Mask R-CNN to generate skull localization. Jing Xhang et al [19] performed regression CNN to measure fetal head circumference, testing four architectures and three regression loss functions. Their experiments showed that Regression ResNet50 combined with mean square error produced the best results. V.Rajinikanth et al [20] applied the Jaya algorithm proposed by Rao [21] to determine the optimal threshold by using Otsu's between class variance and for post-processing and segmentation Chan-Vese to extract the area where the head is located resulting in 88.5% of accuracy. In [22] Mostafa Ghelich Oghli et al used convolutional network architecture MFPUnet for image segmentation. In MFP-Unet feature maps are computed using the entire level of decoder rather than U-net. Then they applied the least square method for ellipse fitting they achieved a 95% dice similarity coefficient. Kirthana. LP et al [23] measured fetal head circumference by using U-net and Hough transform methods.

In [24] Zahra Sobhaninia et al used CNN, their model was based on Link-Net consisting of multi-scale inputs. The system consists of two modules segmentation and Ellipse Tuner. They used three fully connected layers for tuning ellipse parameters which led to improvement in segmentation. In [25], a multi-class segmentation neural network was applied to identify three planes of the fetal head, abdomen, and femur. Then for region fitting, they used two algorithms U-net and Deeplabv3+ with weighted cross entropy and then performed ellipse fitting to segment the head and abdomen. They analyzed Deeplabv3+ performed better and high accuracy in the case of the fetal head than other planes. Tran Tuan Canh et al [26] applied a masked regional-based convolution neural network for estimating fetal head circumference. They modified the existing Mask R-CNN for mask generation, using the fitted ellipse to compute circumference with Ramanujan's formula. Juan J. Cerrolaza et al [27] used two-stage convolution neural networks. In the first stage, they got the initial segmented image and computed two additional channels angle incidence map and shadow casting map which help to reduce fading and shadowing effect. The second stage provides a complete segmented fetal skull and obtained an 83% dice coefficient. Maire Chiara Fiorentino et al [28] developed a

method comprising a region proposal CNN for localization and centering of the fetal head, a regression CNN based on distance fields to find the head circumference line, and ellipse fitting to extract the fetal skull boundary, achieving a dice similarity coefficient of 97.75. Xing Yang et al [29]used FCN architecture with an encoder-decoder design, a hybrid attention scheme used in up sampling, and skip connections for preserving local details and global context for fetal head segmentation. In [30] Siqing Nie et al proposes a deep network DBN and directional edges-based solution to detect fetal head.

Then Hough transform is used for circle detection. Dong hao Qiao and Farhana Zulkermine [31] modify U-net model by adding dilated convolutional layer in last encoder and on skip block use squeeze-and-excitation blocks. Model was trained on HC18 dataset and achieved 97.21 of dice coefficient and 2.27 mm mean absolute difference. Khalid Rasheed et al [32] segmented the fetal head using AlexNet to classify head fragments from ultrasound videos. Annotated UNET architecture is used for localization and segmentation of the fetal skull on selected frames then the least square method is used for ellipse fitting resulting in 96% accuracy. A. Ciurte et al [33] used a method based on their previous work variation non-local semi-supervised approach consisting of continuous min-cut and Pearson distance. They identified the head by fitting two concentric ellipses in the middle of the image but if the head is not in a centered position of the image they use user-assisted labels. Then compute OFD and BPD horizontally and vertically by using an ellipse to calculate the circumference. In a paper [34] Thomas Van den Heuvel et al applied three quantification systems A, B, and C with 1,2, and 3 pipelines respectively. System A is used for training while System B and C pipelines are used for different trimesters. They used Haar-like features for features extraction and Random Forest Classifiers for classification then applied ellipse fitting.

Material and Methods:

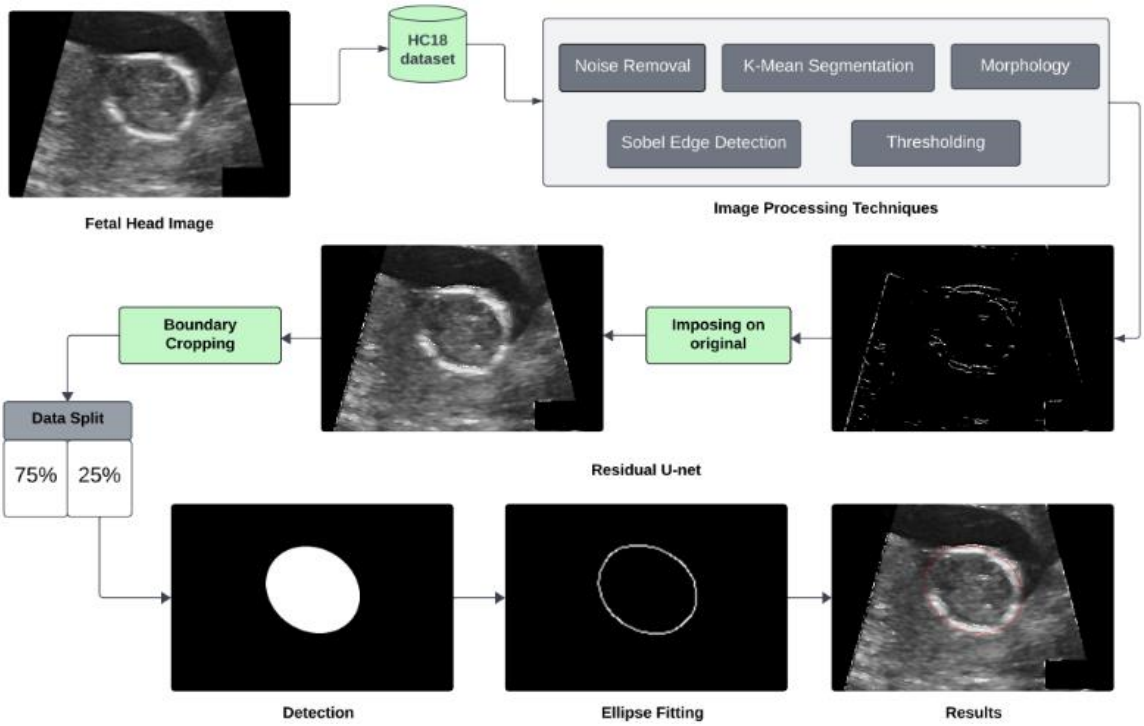

Figure 1. Work Flow of Proposed Solution

After analyzing various solutions as discussed in the literature review and experiments, we have chosen to enhance the accuracy and visual results of fetal head segmentation by combining both image processing and deep learning techniques. Our proposed algorithm consists of two phases: image processing and deep learning. The block diagram of the proposed method is illustrated in Figure 1.

Dataset Description and Preparation:

The dataset used in this study is obtained from a challenge [4] and consists of 1334 two-dimensional ultrasound images captured in the standard plane from the Department of Obstetrics of the Radboud University Medical Center, Nijmegen, and the Netherlands. These images were obtained from 551 pregnant women who underwent routine ultrasound examinations between May 2014 and May 2015. Only images of fetuses without any abnormalities were included in this study. The ultrasound images were recorded by an experienced sonographer using either the Voluson E8 or Voluson 730 ultradevice manufactured by General Electric, Austria. The collection and use of this data for the study were approved by the Regional Ethics Committee (CMO Arnhem-Nijmegen), and informed consent was waived due to the retrospective nature of the data. All data were anonymized according to the tenets of the Declaration of Helsinki.

The dataset contains two sets: a training set, which includes 999 images, and a test set, which includes 335 images. Each image in the dataset has a size of 800 x 540 pixels, and the pixel size ranges from 0.052 to 0.326 mm. The training set also includes manual annotations of the head circumference, which were marked by a trained sonographer, and also their parameter measurements in millimeters are included in a CSV file. The ground truth information for each image is available in the form of labels. However, for training, it is necessary to convert these labels into masks. Masks are binary images that serve to define the boundaries or contours of objects within an image. We used the connected component technique [35] for mask generation which is commonly used in image processing and computer vision tasks. The original images were initially sized at 800×540 pixels. We standardized all images to 800×540 pixels for uniformity, Normalization is applied to scaling pixel values to a standard range like [0, 1].These techniques help mitigate variability in image quality caused by differences in imaging devices, settings, and conditions.

Image Processing:

Within the medical field, image processing [36] involves the examination and manipulation of various types of medical images, including ultrasound images, MRI scans, X-rays, CT scans, and microscopic images. The primary goal of medical image processing is to enhance the quality of medical images by applying specialized technique. These techniques are designed to improve image clarity, remove unwanted noise, and enhance the visibility of critical structures or anomalies within the images. After converting to grayscale, our aim was to identify skull edges.

We applied canny edge detection but it also identifies other boundaries from background particularly in first trimester because of minimal visibility. Same issues were observed with Laplacian and Prewitt operators, which are highly sensitive to noise. Consequently, we move to Sobel filter which yielded better results rather than other techniques. After edge detection, resultant image still have some particles which is not a part of interested region. Here we have three types of region; interested foreground, foreground, and background. To segment these regions effectively, we employed K-means clustering, adjusting the cluster size accordingly. For thresholding, we initially used adaptive and Otsu's thresholds. However, these automated methods sometimes included parts of the background that remained even after K-means segmentation. To address this, we turned to histogram analysis to determine and apply an optimal threshold manually. Furthermore, we fine-tuned the parameters for Morphology and Thinning operations through iterative experiments. This involved testing different kernel sizes, loop counts, and operation sequences to identify the optimal configuration. The selected techniques are discussed in following sections.

Grayscale Conversion and Noise Removal:

Grayscale conversion involves converting a color image into a grayscale version where shades of gray represent the image's pixel. This conversion discards the color information

from the original image and instead represents each pixel based solely on its brightness value. Ultrasound images can experience different forms of noise such as Gaussian noise, Speckle noise, Impulse or Salt-and-Pepper noise, and Ringing Artifacts. Addressing and mitigating these various forms of noise Kumar. N et al [37] highlighted that different filters produce optimal outcomes for various types of noise in images. The median filter [38] proves effective in removing Poisson and Salt and Pepper noise [39]. Additionally, the Gaussian filter [40] demonstrates excellent results when applied to Gaussian Noise images. On the other hand, the Wiener filter [41] surpasses other filters in dealing with Speckle Noise, a ringing artifact. In our approach to reduce noise in ultrasound images, we utilized a combination of median, Gaussian, and Wiener filters for noise reduction.

Sobel Edge Detection:

Sobel filter is a gradient-based technique implemented that calculates the intensity gradient at each pixel in the image [42]. The Sobel filter offers useful insight into the transitions in the image at each pixel by examining the direction of the most significant rise from light to dark and the rate of change in that direction. This technique allows us to evaluate whether changes are rapid or smooth, which helps in determining if a pixel constitutes an edge and identifying the orientation of the edge.

K-Mean Segmentation:

After applying edge detection there are three parts in the image, background, foreground (but not area of interest), and foreground (area of interest). To differentiate these classes, we utilized clustering algorithms, with K-Means being a widely used unsupervised technique specifically designed for segmenting areas of interest from the background. K-Means partitions the given data into K clusters or subsets based on K centroids. In our case, with three classes (background, non-area of interest, and area of interest), we used three clusters. This algorithm is particularly useful when working with unlabeled data to discover distinct groups by identifying similarities or patterns, with the number of groups determined by the value of K.

Thresholding:

Thresholding [43] is a segmentation technique that transforms a grayscale image into a binary image, where each pixel is represented by either 0 or 1. Pixels with intensity values higher than the threshold are assigned the value 1 (white) while the remaining pixels are assigned the value 0 (black). Histogram is computed to select the appropriate thresholding value. We observed that all histograms have three peaks background lies on the black side, foreground lies on the white side, and foreground (but not interest region) near 30 to 50 on the x-axis illustrated in Figure 2. So, we selected 50 as our thresholding value.

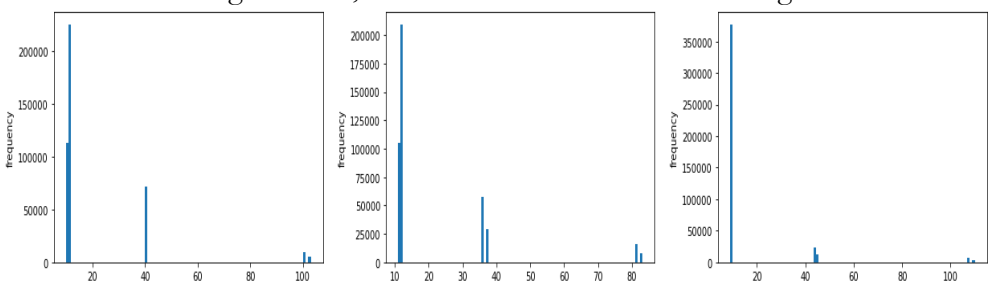

Figure 2. Histogram Analysis

Morphology:

To refine and enhance the fetal head boundaries by addressing disconnected regions and removing small particles surrounding the fetal head, we employed morphological operations. The term "Morphology" refers to a set of image processing techniques used to extract valuable information about region shapes, boundaries, and more [44]. Morphological dilation is a process that fills in small gaps within objects and enhances the visibility of objects. It makes shapes with filling appear more pronounced and lines appear thicker. Closing involves

performing a dilation followed by erosion. It similarly alters the shapes of objects. During the dilation step, nearly connected objects can merge, and even after the subsequent erosion step, they often remain merged.

Thinning:

To extract the head's structural skeleton, we applied a morphological thinning operation. It is used to decrease the width of an object's boundary to a single pixel. It involves iteratively eroding and dilating the image using a specially designed structuring element to remove pixels from the object's boundary. The structuring element acts as a small shape that defines the pixel neighborhood in the image. Morphological thinning finds applications in various image processing tasks, such as the skeletonization of objects, denoising images by reducing unwanted details, and preserving essential features. Results of all image processing techniques are shown in Figure 3.

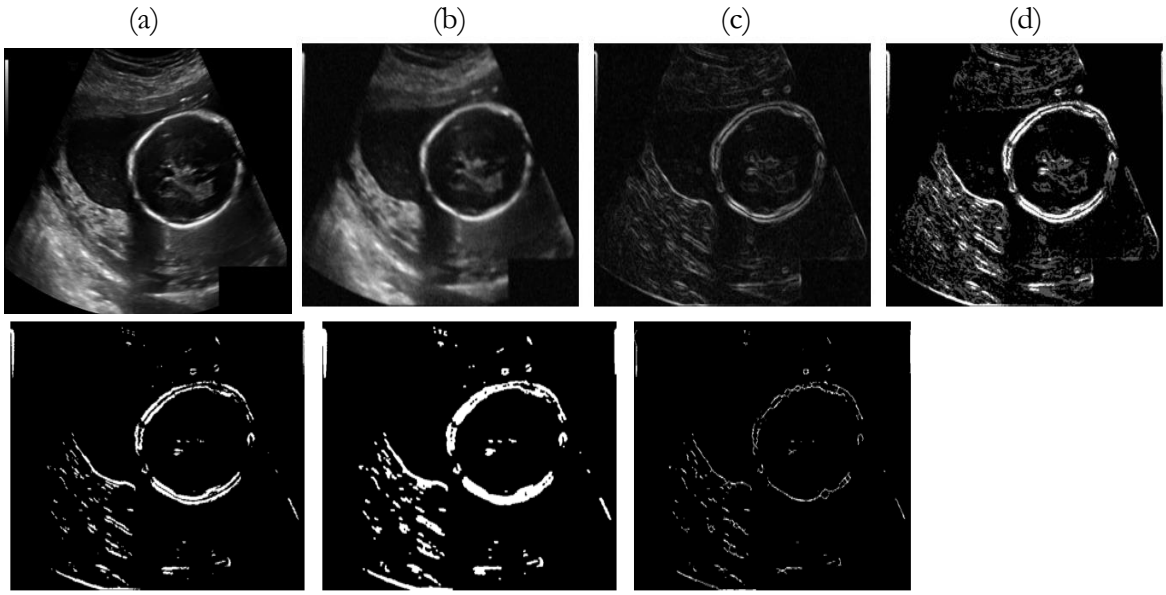

Figure 3. Image Processing (a) Original Image (b) After Pre-processing (c) Sobel Filter (d) K-mean segmentation (e) Thresholding (f) Morphology (g) Final segmented result after applying thinning operation

Deep Learning:

Deep learning is a type of machine learning that uses complex networks of artificial neurons to learn and understand patterns in large amounts of data. It mimics how our brain works to process information and make predictions.

Data Preprocessing:

The segmented images obtained after applying image processing techniques were imposed on the original images. This process enhances the edges of the fetal head, resulting in improved outcomes and desired visualization. Images in our dataset contain unnecessary boundaries which are not a part fetal head and their elimination does not affect ultrasound. Cropping images before training is a widely used technique to eliminate irrelevant or redundant portions from images that do not contribute useful information to the target task. This reduces model complexity and leads to faster and more efficient training processes, quicker model convergence, and experimentation. The size of the original images is 800×540; we cropped it to 768×512. This process did not affect our interest. There are total 999 images in the training set of the HC18 challenge [4]; we split it as 75% for training, 20% for validation, and 5% for evaluating the model performance.

Model validation was conducted using a random shuffle approach where 20% of the dataset was reserved for validation purposes. This method ensures that each validation set is representative of the overall dataset distribution, helping to prevent any bias in the selection of validation data and ensures that the model is tested on diverse samples from the dataset. Data augmentation is a widely used technique to increase the size of a training dataset by modifying the existing dataset. It enables the model to learn invariant and discriminate features that are robust to changes in the data. Data augmentation techniques did not have direct impact on robustness and performance as model performance highly dependent on segmentation. If segmentation region is perfectly extracted without discontinuous points then we will achieve better results and accuracy from model too. But in first two trimesters fetal head is not properly visible in ultrasound images which can cause discontinuous points in fetal skull. To ensure this we had applied noise, rotation and color augmentation but results are not satisfactory. We specifically applied horizontal flipping and vertical flipping to create augmented samples. Horizontal flipping means left to right flip, vertical flipping which is to down flip, vertical flipping of the horizontally flipped images, and horizontal flipping of the vertically flipped images

Residual U-net Model:

The Residual U-net is a Convolution Neural Network (CNN) architecture [45] that builds upon the U-net structure by incorporating residual connections. Residual connections, inspired by residual networks (ResNets), allow for the direct propagation of information from one layer to another, by passing multiple layers. This helps to alleviate the vanishing gradient problem and enables the network to learn more effectively, especially for deeper architectures. The architecture diagram of the residual u-net is also illustrated in Figure 4.

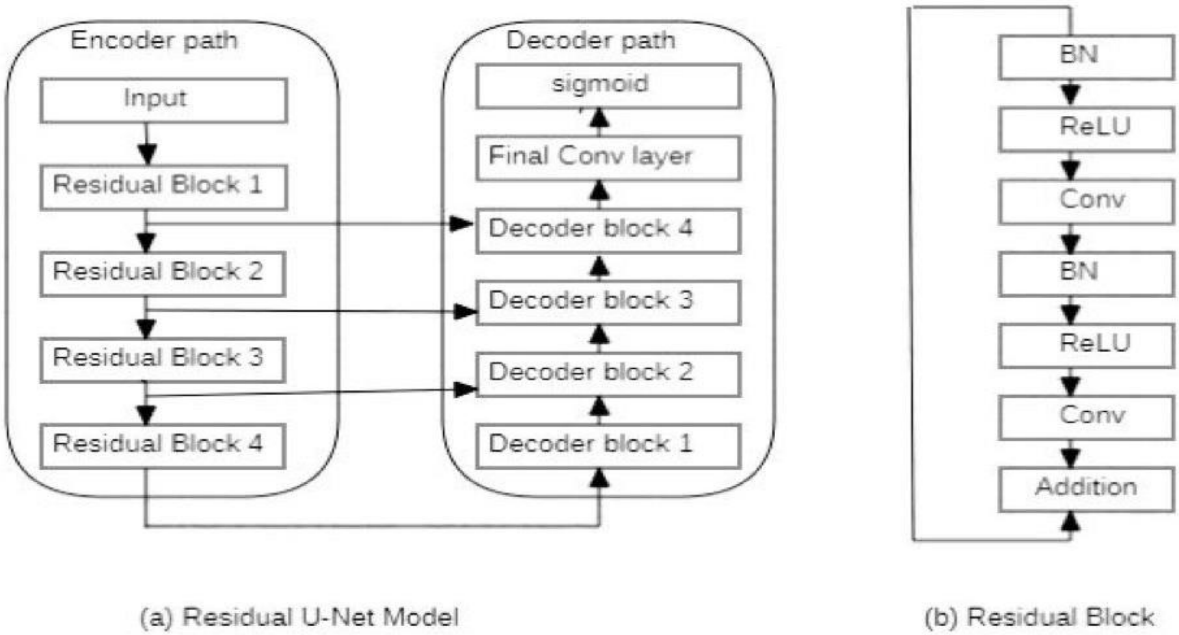

Figure 4. Residual U-Net architecture

The Res U-net architecture [46] comprises an encoder-decoder network with skip connections. The encoder network also referred to as the contracting path consists of multiple convolutional layers followed by activation functions like ReLU. This network gradually reduces the spatial dimensions of the given input image while increasing the number of feature channels. Within each block of the encoder network, residual blocks are employed, which make use of skip connections to enable the direct flow of information from input to output. The bridge or the middle layer of the network connects the encoder and decoder sections. It consists of a convolution layer followed by residual blocks. The decoder network, known as

the expanding path, mirrors the structure of the encoder but in reverse. It employs transpose convolutions to progressively increase the spatial dimensions while decreasing the number of feature channels. The skip connections from the encoder are concatenated with corresponding layers in the decoder, allowing the fusion of low-level and high-level features. Max pooling and dropout operations incorporate dropout regularization, randomly deactivating a percentage of neurons during training to prevent overfitting. The final layer consists of a 1x1 convolution followed by a sigmoid activation function, resulting in a pixel-wise classification output. In the Res U-net, residual connections are added to the traditional U-net structure, enhancing its performance and enabling better feature representation and extraction. This makes the Res U-net well-suited for tasks such as image segmentation, where accurate localization and delineation of objects or boundaries are required.

Post Processing:

In this section, we discussed the steps performed after the model predicts results on the test data. The predicted results are in the form of masks, which were converted from annotations during the training phase. To refine and extract more precise information from these masks, we applied the least square fitting [47] method to fit an ellipse on each labeled region. It minimizes the sum of the square distance between the given data points and their respective points on the fitted ellipse. This method accurately determines the boundary of the fetal head and finds essential measurements like the center, head size, semi-minor axes, semi-major axes, and orientation. With this information, we can predict the head circumference in terms of pixels using the ellipse circumference formula as the head shape is similar to an ellipse. Here, C represents the ellipse circumference while S_a and S_b represent semi-major and semi-minor

$$C = 2\pi\sqrt{\frac{{S_a}^2+{S_b}^2}{2}} \qquad (1)$$

axes respectively. To determine the head circumference in millimeters, we need to multiply the pixel-based circumference values by the provided pixel size. This computation allows us to derive accurate measurements of the head circumference and enhance our understanding of fetal development.

Implementation Details.

The implementation is carried out on the Google Colab platform, utilizing a T4 GPU for accelerated computations. The hardware configuration ensured efficient training and reduced training time. The proposed model was implemented using the TensorFlow and Keras libraries discussed in Table 1. We fine-tuned hyperparameter such as learning rates, batch sizes, epochs, dropout rates, and others through iterative experimentation to optimize segmentation accuracy and biometric measurement accuracy. Batch size 16 yielded the best results among different tested batch sizes (8, 16, and 32). The Adam optimizer consistently performed best in our experiments. After testing learning rates (0.001, 0.0001, 0.00001, and 3e-5), we determined that a learning rate of 3e-5 minimized loss fluctuations during training. A dropout rate of 0.5 was found to be optimal; lower dropout rates led to overfitting. . After experimenting with different number of epochs ranging from 10 to 200, it is found that training with larger number of epochs could lead to overfitting. Hence, to strike a balance between model performance and generalization, 50 epochs were selected as an optimal choice for training the model.

Performance Evaluation Metrics:

The performance of the proposed method is evaluated on the HC18 Grand Challenge dataset; they provided ground truth with a training set annotated by the trained sonographer. We use the Dice Coefficient (DSC), Hausdorff distance (HD), Mean difference (MD), and Mean Absolute difference of Head Circumference (MAD) as performance evaluation metrics.

Table 1. Hardware and software specifications

	For Image Processing	For Residual U-net
Hardware Environment	Core i3 CPU RAM: 8 GB OS: 64-bit GB	T4 GPU RAM: 12GB Disk: 78 GB
Software Environment	Cv2 Numpy Scipy Matplotlib	TensorFlow version 2.12.0, Keras version 2.12.0, and Python version 3.10.12

In our experiments, these measures were essential for evaluating how accurately and precisely our segmentation models performed.The dice coefficient is a widely used parameter for measuring the similarity and overlapping between two sets of images and their ground truth. The Dice coefficient ranges between 0 and 1, where a value of 0 signifies no overlap between the sets, while a value of 1 indicates a perfect match and better accuracy.

$$Dice\ Coefficient = \frac{2*|A \cap B|}{|A|+|B|} \quad (2)$$

Here, A and B represent the two sets of predicted segmentation results and the ground truth, respectively.

. $$Dice\ Loss = 1 - Dice\ Coefficient \quad (3)$$

The Hausdorff distance is a measure of the maximum distance between a point on one boundary and its closest point on the other boundary. A smaller Hausdorff distance suggests a higher level of similarity or better alignment between the two sets, indicating a closer match between the predicted and ground truth boundaries.

$$Hausdorff\ Distance = \max\left(h(A,B), h(A,B)\right) \quad (4)$$

Here A and B are images from the predicted segmentation mask and the ground truth mask which contains several pixels. Where A = $\{a_1 \ldots a_n\}$ and B = $\{b_1 \ldots b_n\}$.

$$h(A,B) = max_{\mathrm{a}\in\mathrm{A}} max_{\mathrm{b}\in\mathrm{B}} \|\mathrm{a} - \mathrm{b}\| \quad (5)$$

The mean difference is the simple difference between a given head circumference and our predicted circumference. Its absolute deviation is referred to as Mean Absolute Difference. Here Gt means ground truth and Pre means predicted.

$$Mean\ difference = HC_{\mathrm{Pre}} - HC_{\mathrm{Gt}} \quad (6)$$

Experiments and Result:

In this section, we presented the visual results obtained after applying the proposed algorithm as well as its performances. The outcomes of the proposed algorithm on the test data sourced from HC18 [4] are shown in Figure 5.The various stages of the algorithm are depicted, including the original test images, their segmented counterparts, and the imposed images, the predicted boundaries generated by the proposed algorithm, the label generation using ellipse fitting, and then results where boundaries are imposed on the test images. When evaluating the proposed technique, it achieved a dice coefficient of 98.12% and a loss of 1.188% on the training dataset. On the validation dataset, it achieved a dice coefficient of 97.99% and a loss of 2.01%. The dice coefficient and loss for each epoch are visualized in Figure 6.In the first graph, it can be observed that the validation loss shows slight fluctuations throughout the 45 epochs but remains consistently below -0.94, which is equivalent to 6%. Towards the later epochs, the validation loss tends to stabilize and align with the training loss.

The second graph displays the dice coefficient for both training and validation on each epoch. Similarly, the validation dice coefficient exhibits slight fluctuations but consistently stays above 94% throughout the 45 epochs. This suggests that the model is learning effectively and does not suffer from overfitting or underfitting. From 45 to 50 epochs, there is close proximity of the training and validation dice coefficients. The similarity indicates that the

model can generalize well to new, unseen data. Throughout the training process, the model's performance on both training and validation sets was monitored closely. This helped identify any signs of overfitting or underfitting, ensuring that the reported results are reliable. To ensure reproducibility, detailed documentation of the experimental setup, including model architecture, hyperparameter, and validation procedure, was maintained. This documentation allows other researchers to replicate the experiments and validate the reported results independently.

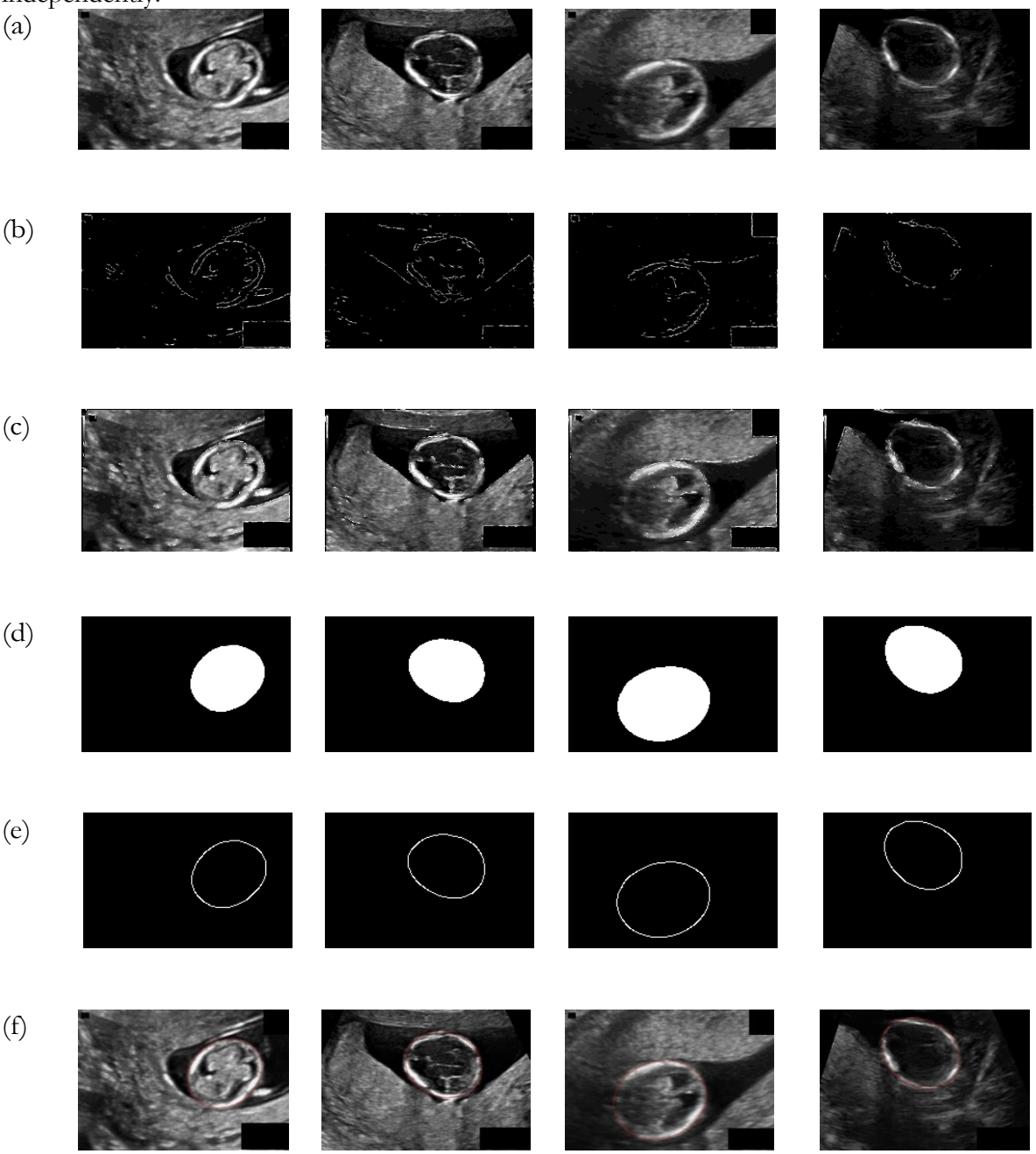

Figure 5. Results of Test data.(a) Original Images,(b) Segmented Images,(c) Imposed Images,(d) Predicted Region (e) Predicted boundaries using connected component,(f) Results drawn on images.

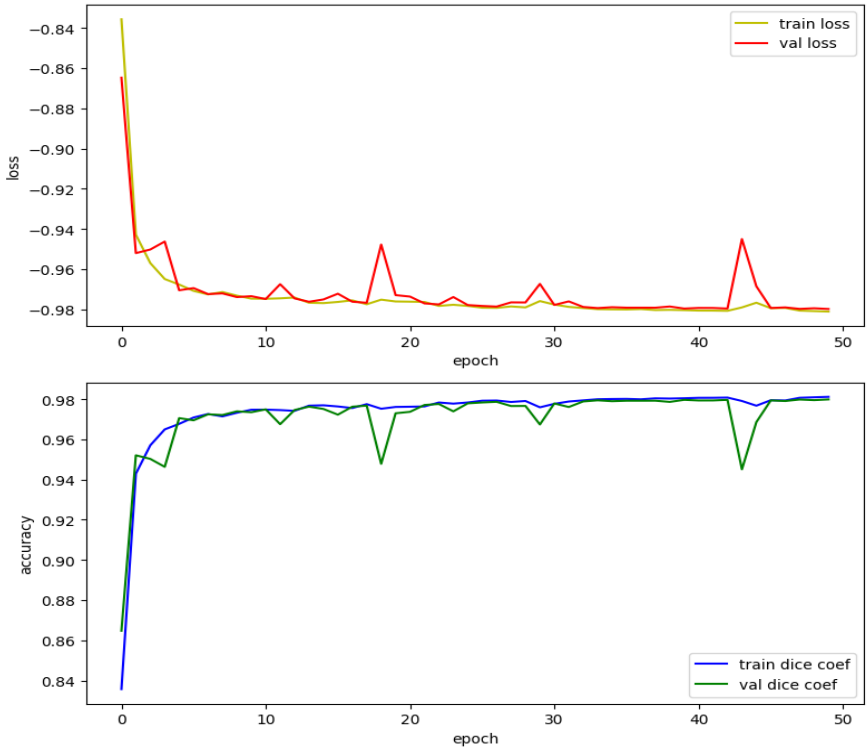

Figure 6. Model Performance: First graph shows loss details and second one shows dice coefficient.

Discussion:

The Residual U-net model also implemented on the original and segmented dataset to evaluated proposed methods performance. In this section, we evaluated and compared our proposed method with two other approaches. In the first approach, we implemented a residual U-Net model on the original images without applying any additional image processing techniques. In the second approach, we applied image processing techniques to enhance the original images before training them on the residual U-Net model. However, we did not impose the obtained mask on the original images. The performance results for each approach are summarized in Table 2 and Table 3. Based on the results shown in Table 2, the model trained on segmented images achieved the lowest dice coefficient of 97.85% using 50 epochs for training and 97.30% for validation. While training dice coefficient of model trained on original and imposed are same 98.12%. However, in terms of validation dice coefficient model trained on imposed images was 97.99%. Table 2 presents the mean difference, mean absolute difference, and mean Hausdorff distance between the head circumference computed on the validation data and the head circumference provided by HC18 [4].

Table 2. Training and Validation dice coefficient and loss of three compared models

Methods	**Training Dice Coefficient (%)**	**Training Loss (%)**	**Validation Dice Coefficient (%)**	**Validation Loss (%)**	**Epochs**
On Original Images	98.12	1.88	97.92	2.08	50
On Segmented Images	97.85	2.15	97.30	2.7	50
On Imposed Images	98.12	1.88	97.99	2.01	50

Table 3. Performance metrics of compared models

Methods	Mean Difference (mm)	Mean Absolute Difference (mm)	Dice Coefficient (%)	Mean Hausdorff Distance (mm)
On Original Images	5.88009	5.90404	97.89	0.57166
On Segmented Images	6.01186	6.47352	97.19	0.65084
On Imposed Images	5.86125	5.89296	97.88	0.56680

According to these evaluations the model trained on imposed images achieved better results because it provides lower mean difference and Hausdorff distance as compared to the other models which indicate the predicted or measured results are closer to the ground truth or reference values. Figure 7 displays test results of the model trained on original images and imposed images, there are noticeable differences in the computation of the fetal skull between the predicted segmentation and the imposed image results. The imposed image yields more acceptable results, with the predicted skull being closer to the actual one while Figure 8 presents testing data results of the segmented trained model and the imposed trained model.

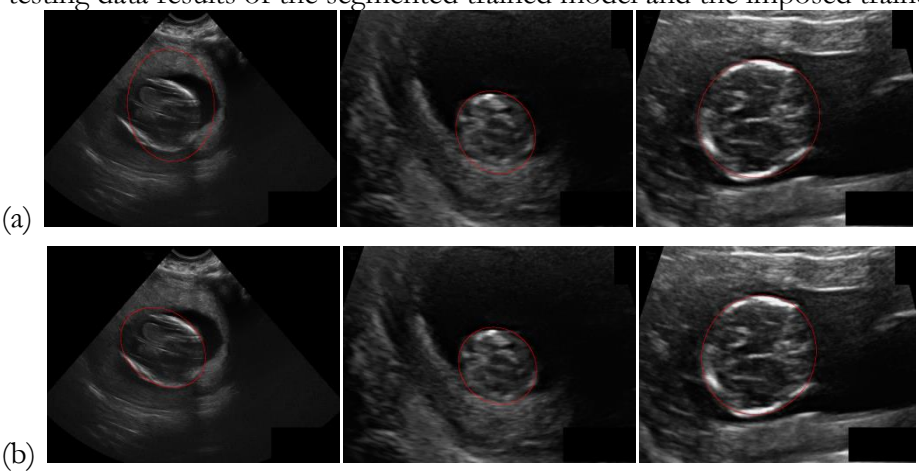

Figure 7. Comparison of Original and Imposed model results. (a) Original Images, (b) Imposed Images

The segmented trained model shows incorrect prediction results because of inadequate detection of edges in the segmentation process whereas the imposed image accurately identifies the skull boundaries.

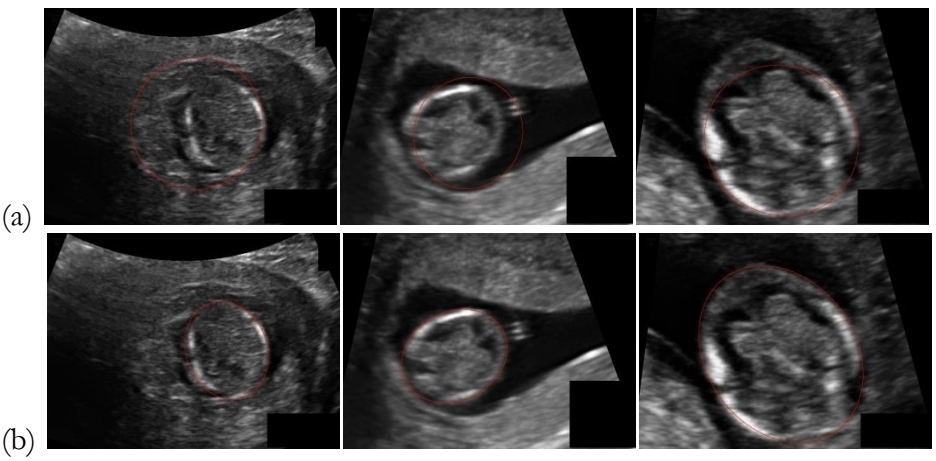

Figure 8. Comparison of Segmented and Imposed model results. (a) Segmented Images, (b) Imposed Images

The dataset includes images from various stages of pregnancy rather than focusing on a specific trimester. However, a limitation is that the current dataset of 999 images may not adequately represent fetal development across all trimesters. Having separate datasets categorized by trimester would enable more precise analysis and performance evaluation for each stage of pregnancy. The proposed Residual U-net model's performance was evaluated against other state-of-the-art approaches, including multi-task network based on link-net architecture (MTLN), Mask-RCNN, random forest classifier, regression CNN, multi-feature pyramid Unet, dilated squeeze and excitation U-net, fast and accurate U-net, using HC18 dataset shown in Table 4. The comparison focused on key metrics essential for evaluating segmentation accuracy and biometric measurement like dice coefficient, hausdorff distance and mean difference. We examined a few existing techniques and then compare their results and performance with our proposed solution. Fiorentino et al [28] suggested region-proposal CNN find the head location and regression CNN for measuring head circumference. They achieve a 1.90 mm mean difference but DSC is 97.76%.

In [22] Mostafa Ghelich Oghli et al used convolutional network architecture MFPUnet for image segmentation in which feature maps are computed using the entire level of decoder rather than U-net. They achieved a 95% dice similarity coefficient. Sobhanimia et al[24]presented Multi-Task deep network that utilizes the Link-Net structure and incorporates multi-scale inputs, without an ellipse tuner. It provides smooth elliptical segmentation results, although their DSC is 96.84% with a 2.21 mm mean absolute difference and 1.72 mm mean HD. Donghao Qiao and Farhana Zulkermine [31] modify U-net model by adding dilated convolutional layer in last encoder and on skip block use squeeze-and-excitation blocks. Model was trained on HC18 dataset and achieved 97.21 of dice coefficient and 2.27 mm mean absolute difference. Thomas et al [34] applied a random forest classifier for head localization using haar-like features and Hough transform for ellipse fitting with 97% DSC and 2.8 mm mean absolute difference but their mean HD is 1.32 mm. Proposed model with dice coefficient of 97.99% outperformed the other state-of-the-art methods.

Table 4. Performance comparison with state-of-art-solutions using HC18 dataset

Authors	**Year**	**Dice Coefficient (%)**	**Mean Difference (mm)**	**Mean Absolute difference (mm)**	**Mean Hausdorff distance (mm)**	**Data-set**
Fiorentino et al [28]	2022	97.76	0.21	1.90	1.32	HC18
DonghaoQiao [31]	2020	97.24	-	2.27	-	HC18
Thomas et al [34]	2019	97	0.6	2.8	2.0	HC18
Oghli et al [22]	2020	95	-	-	4.5	HC18
Sobhaninia et al [24]	2019	96.84	1.13	2.12	1.72	HC18
Ashkani et al [48]	2022	97.14	-	-	10.09	MFP, HC18
Tran et al [26]	2021	97	7.15	-	-	HC18
Proposed Model	2023	97.99	5.86	5.89	0.56	HC18

Conclusion:

In this study, we proposed an automated solution for estimating fetal head circumference which used variant of U-net (residual u-net) with some image processing techniques to maximize its accuracy. The results obtained from the method demonstrated accurate detection of the head contour, indicating its effectiveness in fetal head circumference estimation. When compared to the ground truth, the proposed method provides a 97.99% of dice coefficient and

0.56 mm of mean Hausdorff distance. Although our proposed method shows promising results in estimating fetal head circumference, there is room for improvement. Some images still exhibit results outside of the fetal skull, indicating the need for further refinement. In future research, we aim to enhance this method and extend its application to other datasets as well.

Acknowledgement. We are grateful to the Grand Challenge for providing the HC18 dataset, which was obtained from the free and open-source Zenodo database. This dataset has been essential to the development and accomplishment of this study.

Conflict of interest. The authors declare no conflicts of interest.

Ethics approval and consent to participate. Formal consent is not required in this type of study.

Availability of dataset and materials. The data used in this research are available in the HC18 repository and can be obtained from https://zenodo.org/records/1327317, Accessed: 2023.

Author's Contribution. A.S. and Z.S. conceived the idea and designed the algorithm. A.S. carried out experiments and wrote the main manuscript text. M.D. organized and finalized the manuscript. A.S., Z.S., and M.D. performed validation and discussion. Z.S. supervised the research. All authors have proofread the manuscript.

References:

[1] D. L. Miller, "Safety Assurance in Obstetrical Ultrasound," *Semin. Ultrasound, CT MRI*, vol. 29, no. 2, pp. 156–164, Apr. 2008, doi: 10.1053/J.SULT.2007.12.003.

[2] J. Espinoza, S. Good, E. Russell, and W. Lee, "Does the Use of Automated Fetal Biometry Improve Clinical Work Flow Efficiency?," *J. Ultrasound Med.*, vol. 32, no. 5, pp. 847–850, May 2013, doi: 10.7863/JUM.2013.32.5.847.

[3] J. Lanowski *et al.*, "Impact of Ultrasound Training and Experience on Accuracy regarding Fetal Weight Estimation at Term Creative Education," *Creat. Educ.*, vol. 8, no. 11, pp. 1761–1773, Sep. 2017, doi: 10.4236/CE.2017.811120.

[4] "Automated measurement of fetal head circumference", doi: 10.5281/ZENODO.1322001.

[5] "R. Ramya, K. Srinivasan, K. P. Devi, S. Preethi,... - Google Scholar." Accessed: Aug. 07, 2024. [Online]. Available: https://scholar.google.com/scholar?hl=en&as_sdt=0%2C5&q=R.+Ramya%2C+K.+Srinivasan%2C+K.+P.+Devi%2C+S.+Preethi%2C+and+G.+Poonkuzhali%2C+"Prenatal+fetal+weight+detection+using+image+processing"%2C+International+Journal+of+Scientific+%26+Technology+Research+2018%3B+7%3A+37–39&btnG=

[6] R. Monica, K. Nirmala, V. J. Kumar, and B. Divya, "Assessment of fetal biometry using ultrasound images," *Proc. 2020 IEEE Int. Conf. Adv. Dev. Electr. Electron. Eng. ICADEE 2020*, Dec. 2020, doi: 10.1109/ICADEE51157.2020.9368917.

[7] T. James and S. Thomas, "Segmentation of Head from Ultrasound Fetal Image using Chamfer Matching and Hough Transform based Approaches", Accessed: Aug. 06, 2024. [Online]. Available: www.ijert.org

[8] W. Lu, J. Tan, and R. C. Floyd, "Fetal head detection and measurement in ultrasound images by an iterative randomized Hough transform," *https://doi.org/10.1117/12.533073*, vol. 5370, pp. 557–565, May 2004, doi: 10.1117/12.533073.

[9] K. Thirusittampalam and J. Thangavel, "Fetal Head Detection in 2D Ultrasound Images using Deep Learning," 2020, Accessed: Aug. 06, 2024. [Online]. Available: http://repo.lib.jfn.ac.lk/ujrr/handle/123456789/3804

[10] "C. Sun, "Automatic fetal head measurements from... - Google Scholar." Accessed: Aug. 07, 2024. [Online]. Available:

https://scholar.google.com/scholar?hl=en&as_sdt=0%2C5&q=C.+Sun%2C+"Automatic+fetal+head+measurements+from+ultrasound+images+using+circular+shortest+paths".+Proceedings+of+challenge+US%3A+biometric+measurements+from+fetal+ultrasound+images%2C+ISBI+2012%2C+13–15&btnG=

[11] "A multilevel thresholding combined with edge detection and shape-based recognition for segmentation of fetal ultrasound images | Request PDF." Accessed: Aug. 06, 2024. [Online]. Available: https://www.researchgate.net/publication/312455757_A_multilevel_thresholding_combined_with_edge_detection_and_shape-based_recognition_for_segmentation_of_fetal_ultrasound_images

[12] V. Salari, I. Zador, L. Chik, and R. J. Sokol, "Automated measurements of fetal head from ultrasound images," *https://doi.org/10.1117/12.18907*, vol. 1233, pp. 213–216, Jul. 1990, doi: 10.1117/12.18907.

[13] Y. Shen, J. Yu, Y. Shen, and Y. Wang, "Fetal skull analysis in ultrasound images based on iterative randomized Hough transform," *https://doi.org/10.1117/12.811431*, vol. 7265, pp. 143–151, Mar. 2009, doi: 10.1117/12.811431.

[14] R. Xu, J. Ohya, B. Zhang, Y. Sato, and M. G. Fujie, "Automatic Fetal Head Detection on Ultrasound Images by An Improved Iterative Randomized Hough Transform", Accessed: Aug. 07, 2024. [Online]. Available: https://www.researchgate.net/publication/303723203

[15] W. Fathima Farsana, "AutomaticFetal Head Circumference Measurement in 2D Ultrasound Fetal Images using Histogram of Oriented Gradient," *Int. J. Adv. Res. Eng. Technol.*, vol. 11, no. 12, pp. 484–491, 2020, doi: 10.34218/IJARET.11.12.2020.052.

[16] "Automatic image quality assessment and measurement of fetal head in two-dimensional ultrasound image." Accessed: Jul. 21, 2024. [Online]. Available: https://www.spiedigitallibrary.org/journals/journal-of-medical-imaging/volume-4/issue-02/024001/Automatic-image-quality-assessment-and-measurement-of-fetal-head-in/10.1117/1.JMI.4.2.024001.full#_=_

[17] K. D. Rahayu, R. Sigit, and D. Agata, "Fetal head and femur detection from USG image to estimate gestational age," *Int. Electron. Symp. Knowl. Creat. Intell. Comput. IES-KCIC 2018 - Proc.*, pp. 242–247, Jul. 2018, doi: 10.1109/KCIC.2018.8628560.

[18] B. Al-Bander, T. Alzahrani, S. Alzahrani, B. M. Williams, and Y. Zheng, "Improving Fetal Head Contour Detection by Object Localisation with Deep Learning," *Commun. Comput. Inf. Sci.*, vol. 1065 CCIS, pp. 142–150, 2020, doi: 10.1007/978-3-030-39343-4_12.

[19] J. Zhang, C. Petitjean, P. Lopez, and S. Ainouz, "Direct estimation of fetal head circumference from ultrasound images based on regression CNN," *Proceedings of Machine Learning Research*, vol. 121. PMLR, pp. 914–922, Sep. 21, 2020. Accessed: Aug. 06, 2024. [Online]. Available: https://proceedings.mlr.press/v121/zhang20a.html

[20] V. Rajinikanth, N. Dey, R. Kumar, J. Panneerselvam, and N. Sri Madhava Raja, "Fetal Head Periphery Extraction from Ultrasound Image using Jaya Algorithm and Chan-Vese Segmentation," *Procedia Comput. Sci.*, vol. 152, pp. 66–73, Jan. 2019, doi: 10.1016/J.PROCS.2019.05.028.

[21] R. V. Rao, "Jaya: A simple and new optimization algorithm for solving constrained and unconstrained optimization problems," *Int. J. Ind. Eng. Comput.*, vol. 7, pp. 19–34, 2016, doi: 10.5267/j.ijiec.2015.8.004.

[22] M. G. Oghli *et al.*, "Automatic Measurement of Fetal Head Biometry from Ultrasound Images using Deep Neural Networks," *2020 IEEE Nucl. Sci. Symp. Med. Imaging Conf. NSS/MIC 2020*, 2020, doi: 10.1109/NSS/MIC42677.2020.9507932.

[23] K. Lp and Muthurasu N, "AUTOMATIC ESTIMATION OF FETAL HEAD

CIRCUMFERENCE USING UNET AND HOUGH TRANSFORM," *Int. Res. J. Eng. Technol.*, 2020, Accessed: Aug. 07, 2024. [Online]. Available: www.irjet.net

[24] Z. Sobhaninia *et al.*, "Fetal Ultrasound Image Segmentation for Measuring Biometric Parameters Using Multi-Task Deep Learning," *Proc. Annu. Int. Conf. IEEE Eng. Med. Biol. Soc. EMBS*, pp. 6545–6548, Jul. 2019, doi: 10.1109/EMBC.2019.8856981.

[25] S. Bano *et al.*, "AutoFB: Automating Fetal Biometry Estimation from Standard Ultrasound Planes," *Lect. Notes Comput. Sci. (including Subser. Lect. Notes Artif. Intell. Lect. Notes Bioinformatics)*, vol. 12907 LNCS, pp. 228–238, 2021, doi: 10.1007/978-3-030-87234-2_22.

[26] T. T. Canh, T. D. Toan, L. M. Hung, and T. Van Lang, "AN AUTOMATIC SYSTEM FOR ESTIMATING FETUS HEAD CIRCUMFERENCE USING 2D ULTRASOUND IMAGES," Dec. 2021, doi: 10.15625/VAP.2021.0055.

[27] J. J. Cerrolaza *et al.*, "Deep learning with ultrasound physics for fetal skull segmentation," *Proc. - Int. Symp. Biomed. Imaging*, vol. 2018-April, pp. 564–567, May 2018, doi: 10.1109/ISBI.2018.8363639.

[28] M. C. Fiorentino, F. P. Villani, M. Di Cosmo, E. Frontoni, and S. Moccia, "A review on deep-learning algorithms for fetal ultrasound-image analysis," *Med. Image Anal.*, vol. 83, p. 102629, Jan. 2023, doi: 10.1016/J.MEDIA.2022.102629.

[29] X. Yang *et al.*, "Hybrid attention for automatic segmentation of whole fetal head in prenatal ultrasound volumes," *Comput. Methods Programs Biomed.*, vol. 194, p. 105519, Oct. 2020, doi: 10.1016/J.CMPB.2020.105519.

[30] S. Nie, J. Yu, P. Chen, J. Zhang, and Y. Wang, "A novel method with a deep network and directional edges for automatic detection of a fetal head," *2015 23rd Eur. Signal Process. Conf. EUSIPCO 2015*, pp. 654–658, Dec. 2015, doi: 10.1109/EUSIPCO.2015.7362464.

[31] D. Qiao and F. Zulkernine, "Dilated Squeeze-and-Excitation U-Net for Fetal Ultrasound Image Segmentation," *2020 IEEE Conf. Comput. Intell. Bioinforma. Comput. Biol. CIBCB 2020*, Oct. 2020, doi: 10.1109/CIBCB48159.2020.9277667.

[32] K. Rasheed, F. Junejo, A. Malik, and M. Saqib, "Automated Fetal Head Classification and Segmentation Using Ultrasound Video," *IEEE Access*, vol. 9, pp. 160249–160267, 2021, doi: 10.1109/ACCESS.2021.3131518.

[33] A. Ciurte *et al.*, "Semi-supervised segmentation of ultrasound images based on patch representation and continuous min cut," *PLoS One*, vol. 9, no. 7, Jul. 2014, doi: 10.1371/JOURNAL.PONE.0100972.

[34] T. L. A. van den Heuvel, H. Petros, S. Santini, C. L. de Korte, and B. van Ginneken, "Automated Fetal Head Detection and Circumference Estimation from Free-Hand Ultrasound Sweeps Using Deep Learning in Resource-Limited Countries," *Ultrasound Med. Biol.*, vol. 45, no. 3, pp. 773–785, Mar. 2019, doi: 10.1016/j.ultrasmedbio.2018.09.015.

[35] "Image Analysis - Connected Components Labeling." Accessed: Aug. 07, 2024. [Online]. Available: https://homepages.inf.ed.ac.uk/rbf/HIPR2/label.htm

[36] "Image Processing - an overview | ScienceDirect Topics." Accessed: Aug. 07, 2024. [Online]. Available: https://www.sciencedirect.com/topics/computer-science/image-processing

[37] N. Kumar and M. Nachamai, "Noise Removal and Filtering Techniques Used in Medical Images," *Orient. J. Comput. Sci. Technol.*, vol. 10, no. 1, pp. 103–113, Mar. 2017, doi: 10.13005/OJCST/10.01.14.

[38] "Spatial Filters - Median Filter." Accessed: Aug. 07, 2024. [Online]. Available: https://homepages.inf.ed.ac.uk/rbf/HIPR2/median.htm

[39] "An introduction to image segmentation with k-means clustering", [Online]. Available:

https://www.kdnuggets.com/k-means-clustering.html
[40] "Spatial Filters - Gaussian Smoothing." Accessed: Aug. 07, 2024. [Online]. Available: https://homepages.inf.ed.ac.uk/rbf/HIPR2/gsmooth.htm
[41] "Image pyramids and the laplacian", [Online]. Available: https://www.owlnet.rice.edu/wiener.html
[42] "Sobel edge detection", [Online]. Available: https://www.imageeprocessing.com/2011/12/sobel-edge-detection.html
[43] "Image Processing with Python: Thresholding." Accessed: Jul. 21, 2024. [Online]. Available: https://datacarpentry.org/image-processing/07-thresholding.html
[44] "Types of Morphological Operations - MATLAB & Simulink." Accessed: Jul. 21, 2024. [Online]. Available: https://www.mathworks.com/help/images/morphological-dilation-and-erosion.html
[45] Z. Li, F. Liu, W. Yang, S. Peng, and J. Zhou, "A Survey of Convolutional Neural Networks: Analysis, Applications, and Prospects," *IEEE Trans. Neural Networks Learn. Syst.*, vol. 33, no. 12, pp. 6999–7019, Dec. 2022, doi: 10.1109/TNNLS.2021.3084827.
[46] "Attention U-Net, ResUnet, U-Net++, U^2-Net | AIGuys." Accessed: Jul. 21, 2024. [Online]. Available: https://medium.com/aiguys/attention-u-net-resunet-many-more-65709b90ac8b
[47] G. Zhou, K. Zhong, Z. Li, and Y. Shi, "Direct Least Absolute Deviation Fitting of Ellipses," *Math. Probl. Eng.*, vol. 2020, no. 1, p. 1317349, Jan. 2020, doi: 10.1155/2020/1317349.
[48] V. Ashkani Chenarlogh *et al.*, "Fast and Accurate U-Net Model for Fetal Ultrasound Image Segmentation," *Ultrason. Imaging*, vol. 44, no. 1, pp. 25–38, Jan. 2022, doi: 10.1177/01617346211069882/ASSET/IMAGES/LARGE/10.1177_01617346211069882-FIG6.JPEG.